

Toward a mobile crowdsensing system for road surface assessment

Xiao Li*, Daniel W. Goldberg

Department of Geography, Texas A&M University, 3147 TAMU, College Station, TX 77843-3147, United States

ARTICLE INFO

Keywords:

Road surface roughness
Crowdsensing
Smartphone
Transient events detection

ABSTRACT

Road surface roughness assessment plays an important role in transportation infrastructure management. Many approaches have been proposed to assess road surface conditions, however, most of these are either labor-intensive tasks or make use of specialized and expensive instruments. The concept of “citizen sensing”, which takes advantages of the sensor-rich smartphones, has been employed by scientists because of its low-cost and high-efficiency. This paper presents a novel crowdsensing-based system for road surface assessment using smartphones. The built-in GPS receiver and an accelerometer in smartphones are utilized to capture a spatial series of the geo-referenced Z-axis accelerations of the road surface, which are used to compute two assessment indexes that aid in determining the road quality. Field tests of the proposed system demonstrate that the condition of the road surface can be effectively identified and the transient events can be properly detected and located by mining the crowd sensed data.

1. Introduction

Road surface roughness has been assessed as a significant factor in road maintenance, management, and construction. Road surface transient events, such as potholes and bumps, not only impact road quality but also affect driver safety, fuel consumption and road maintenance (Beuving, De Jonghe, Goos, Lindahl, & Stawiarski, 2004; Vittorio et al., 2014). The World Bank has identified road roughness as a primary factor in the analysis of road quality vs. user cost. Many studies have demonstrated that the improvement of road surface conditions could directly promote fuel efficiency as well as driving safety (Beuving et al., 2004; Vittorio et al., 2014).

Studies have been carried out on the road surface roughness assessment since the 1950s. Several approaches, which require the use of costly and sophisticated vehicular instruments have been proposed and widely accepted, such as using laser profilometers to calculate the international roughness index (Paterson & Attoh-Okine, 1992; Watanatada, 1987), computing deflection basin parameters by deflectometers (Kim, 2001; Xu, Ranji Ranjithan, & Richard Kim, 2002) or using ground penetrating radar to determine the conditions of the roads (Cao, Labuz, & Guzina, 2011). However, these traditional assessment methods are labor-intensive and time-consuming requiring professional knowledge and high-end instrumentation (Harrison & Park, 2008). Most local governments and small municipalities cannot afford the high cost of these methods with a limited budget.

New detection methods have been proposed over the past few years, which can achieve a higher road revisiting rate and lower equipment

cost (Allouch, Koubaa, Abbes, & Ammar, 2017; Astarita et al., 2012; Bhoraskar, Vankadhara, Raman, & Kulkarni, 2012; Eriksson et al., 2008; Macias, Suarez, & Lloret, 2013). These methods are used to monitor the ever-changing road surfaces by extracting the road surface anomalies and their corresponding locations. With various sensor technologies and the powerful computing capabilities, the use of smartphone sensing in research is proliferating. Smartphones equipped with a number of built-in sensors can be used to support various customized applications, which have been identified as promising platforms and can be used for mobile geospatial computing (Chen & Guinness, 2014). Built-in smartphone accelerometers have been utilized to detect ground vehicle jitters caused by the non-flatness of the road surface (Bhoraskar et al., 2012; Chen & Guinness, 2014). More importantly, by combining the accelerometer and GPS data obtained from a smartphone, the road roughness can be automatically geo-referenced (Aleadelat & Ksaibati, 2017; Astarita et al., 2012; Das, Mohan, Padmanabhan, Ramjee, & Sharma, 2010; Eriksson et al., 2008; Perttunen et al., 2011).

1.1. Related work

Threshold techniques have been broadly used to extract road surface transient events. A real-time pothole detection system was designed by Mednis, Strazdins, Zviedris, Kanonirs, and Selavo (2011). Four different transient events detection techniques were compared in this study. The system is designed mainly based on threshold technique. The overall accuracy can reach 90%. Harikrishnan and Gopi (2017)

* Corresponding author.

E-mail address: xiao.li@tamu.edu (X. Li).

applied Gaussian Model on the Z-axis readings of built-in smartphone accelerometer for detecting and classifying bumps and potholes. The research hypothesis is that the Z-axis acceleration should fit on a Gaussian distribution. In this study, the vehicle vibration data was collected from a horizontally fixed smartphone and segmented into groups. A newly designed Max-Abs filter was applied on the segmented data for minimizing the small acceleration spikes and highlighting the abnormal events. Threshold technique was applied to classify the abnormal events as potholes and bumps. The accuracy of detection and classification of this method can up to be 100%.

Several studies investigated the relationship between road surface roughness and accelerometer readings. Amador-Jiménez and Matout (2014) have proposed a low-cost solution for road surface evaluation using tablets' built-in accelerometer. In this study, the Root Mean Square (RMS) of the Z-axis acceleration normalized by vehicle speed was confirmed as a proxy for the International Roughness Index (IRI), which can be used to examine the road quality. Aleadelat and Ksaibati (2017) tested the relationship between the Z-axis acceleration and the present serviceability index (PSI). PSI is a widely-used index for assessing pavement condition. In this study, two smartphones were horizontally fixed on the vehicle's dashboard. An Android app "AndroSensor" was used for data collection at two driving speeds: 40 mph and 50 mph. The result demonstrates that the Z-axis acceleration has a strong linear relationship with PSI.

Many different machine learning methods have also been employed for assessing road surface condition. Eriksson et al. (2008) proposed a signal processing and machine learning based approach to extract potholes from the readings of external GPS and accelerometer. 7 taxis were used in the test for data collection. Sensors were fixed at different positions inside the vehicle. The result demonstrated the pothole and other transient events can be effectively identified by the proposed method. Perttunen et al. (2011) proposed a solution to extract road surface anomalies (e.g. pothole, bumps) from acceleration data and GPS readings. Kalman filter was implemented to reduce the noise of GPS signal. A spectral analysis was performed on the acceleration signal to extract road features. Support Vector Machine (SVM) was used to predict three categories of transient events (i.e., speed bump, bump, and large pothole). Bhoraskar et al. (2012) designed a traffic monitoring system, which uses the detected braking events and vertical acceleration peaks to estimate the traffic congestion and examine potholes. To translate the acceleration from the frame of the portable device to the frame of the vehicle, a 3-axis accelerometers re-orientation was carried out in the system. SVM and K-means Clustering were implemented to predict road surface condition (identified as "bumpy road" or "smooth road") and optimize the assessment result of each road segment. Singh, Bansal, Sofat, and Aggarwal (2017) proposed a new method to detect bumps and potholes using smartphone sensors. An Android app "Smart-Patrolling" was created and employed for data collection. Five filters (Speed, Virtual Re-Orientation, Filtering Z-axis, SMA and Band-Pass filter) and Dynamic Time Warping (DTM) techniques are applied. In this study, smartphones were fixed inside the vehicle at different places including front dashboard pilot, front dashboard co-pilot, and back seat. The ground truth (unique patterns of accelerometer readings corresponding to these bumps and potholes) was collected during training phase and used as the template references. The accuracy of this method for detecting potholes and bumps is 88.66% and 88.89%. Allouch et al. (2017) implemented a machine learning method to estimate road surface condition. An Android app "Road Data Collector" is created for data. In the training phase, the real road quality was manually labeled as "Smooth" or "Potholed" using designed smartphone app. Different road segments' features were extracted from the readings of accelerometer and gyroscope. Correlation-based Feature Selection (CFS) approach was applied to the training dataset to optimize the feature selection. Three different machine learning methods (C4.5 Decision Tree, Support Vector Machines, and Naïve Bayes) were tested in this study. The result demonstrated that

C4.5 classifier has the best performance with an overall accuracy of 98.6%.

Utilizing a crowdsensing method to obtain road surface roughness data would be exceptionally beneficial, as it would allow the data to be frequently updated, resulting in more accurate result, and would involve a minimal cost for local governments. Some researchers have tried to design a crowdsensing system, which can continuously monitor the changes of road surface condition. Chen, Lu, Tan, and Wu (2013) designed a system called CRSM, which has the potential to detect the potholes and assess the road surface quality effectively. This approach takes advantages of the crowd sensed data by utilizing specialized hardware modules (low-cost GPS receiver and accelerometer) mounted on the vehicles. A lightweight data mining approach was employed in this system with 100 taxis recruited for data collection. The accuracy of this system is about 90%. Lima, Amorim, Pereira, Ribeiro, and Oliveira (2016) proposed a simple lightweight smartphone-based approach, which can recognize road quality as "Good", "Normal", "Bad", and "Terrible". This study makes use of threshold technique with a bunch of thresholds are set through the empirical tests to recognize road quality. This study performed a crowdsourcing solution. Crowd sensed results were simply averaged and then mapped using GoogleMaps API.

A comparison of existing methods is detailed in Table 1, which reflects the following problems that need to be addressed: 1) the repeatability of threshold-based methods is limited. Thresholds need to be adjusted and retested when applied under different conditions; 2) machine learning methods require an extensive training phase, which is time-consuming and not suitable for the crowdsensing system; 3) most studies just focus on the transient events detection. A comprehensive road surface assessment is lacking; 4) very few studies utilize crowdsensing approaches, which just simply averages the crowd sensed data. An improved crowdsensing solution for assessing road surface condition need to be further explored.

1.2. Key contributions

This study presents a preliminary mobile crowdsensing system for road surface roughness detection, which includes a mobile data-collecting component and a web-based data server component. It takes advantages of previous studies but differs in following three aspects: 1) **a detailed crowdsensing solution**: An iOS app *Crowdsense* and an Android app *AndroSensor* are utilized in this study for data collection. This paper provides **a detailed result optimization by integrating crowd sensed data**; 2) **with comprehensive road condition assessment**: Instead of just focusing on the pothole or bump detection, a more comprehensive assessment of road conditions is introduced including an overall road condition estimation, IRI-proxy calculation, and transient events (bumps/potholes) detection; 3) **a cloud-based data server**: A low-cost, lightweight, cloud-based system framework, which takes advantages of free Google services, is developed in the study. Google Fusion Table is tested and **innovatively applied in the model for data visualization**.

To verify the proposed solution, a preliminary model for crowdsensing road surface roughness is created, and a detailed experiment is designed and conducted in the city of College Station, Texas.

2. Methodology

This section discusses the research methodologies. First, the system architecture is introduced. The strategy of the proposed road surface assessment is elaborated upon. A detailed explanation of the mathematical algorithm, which is used for evaluating road surface conditions and computing two assessment indexes, is also given in this section. The rest of this chapter covers the result optimization, visualization, and publication.

Table 1
Comparison of existing methods.

	Method	Smartphone sensors	Roughness assessment	Pothole & bump detection	Crowd-sensing	Accuracy
Mednis et al. (2011)	Threshold (Z-Threshold, Z-Diff, STDEV, G-Zero)	Accelerometer, GPS	No	Yes	No	TP = 90% (Pothole)
Harikrishnan & Gopi (2017)	Threshold, Gaussian Model, & A newly designed Max-Abs filter	Accelerometer, GPS	No	Yes	NO	TP = 100% (Pothole)
Amador-Jiménez & Matout (2014)	Threshold	Tablet Accelerometer (Not phone sensors)	Predict IRI using Z-axis Acceleration	No	No	Produce a repeatable indicator of road condition
Aleadelat & Ksaibati (2017)	Exponential Transformation & Simple Linear Model	Accelerometer	Predict PSI using Z-axis Acceleration	No	No	Z-acceleration has a strong liner relationship with and can be used to predict PSI FP < 0.2% (Pothole)
Eriksson et al. (2008)	Signal processing and machining learning based approach	External GPS, Accelerometer (Not phone sensors)	No	Yes	No	FPR = 3% FNR = 18% (Potholes)
Perttunen et al. (2011)	Spectral Analysis & SVM	Accelerometer, GPS	No	Yes	No	FPR = 0% FNR = 10% (Potholes)
Bhoraskar et al. (2012)	K-means Clustering & SVM	Accelerometer, GPS, Magnetometer	"Smooth" Or "Bumpy"	Yes	No	TP (Pothole, Bump) = 88.66%, 88.89%.
Singh et al. (2017)	DTM	Accelerometer, GPS	No	Yes	No	Accuracy = 98.6% (Pothole)
Allouch et al. (2017)	Machine Learning (C4.5 Decision Tree, SVM, and Naïve Bayes)	Accelerometer, Gyroscope	"Smooth" or "Potholed"	Yes	No	Accuracy = 90% (Pothole); Can evaluate road roughness levels correctly
Chen et al. (2013)	Improved Gaussian Mixture Model; Threshold	Hardware modules (Not phone sensors)	"Good", "Fair", "Poor", "Bad"	Yes	Average Crowd Sensed Results	Not reported
Lima et al. (2016)	Threshold	Accelerometer, GPS	"Good", "Normal", "Bad", "Terrible"	Yes	Average Crowd Sensed Results	

2.1. System architecture

In this paper, a crowdsensing approach was employed to assess road surface conditions. The whole system mainly includes two components: a mobile data-collecting component and a web-based data server component as shown in Fig. 1. The mobile data-collecting component requires a user to run the mobile application *AndroSensor* in an Android smartphone or the mobile application *Crowdsense* in an iOS smartphone. Smartphones are used to collect the raw data in real-time including the GPS positions and the raw measurements of the accelerometer and upload the road surface conditions to a cloud-based data server. The server periodically processes the road roughness information contributed from different crowdsourcers and integrates the detection results accordingly.

2.2. Real-time road surface condition assessment

The process of road surface assessment is described in Fig. 2. It consists of four steps: data collection, data process, data integration and assessment indexes calculation.

2.2.1. Accelerometer reorientation

Microelectromechanical systems (MEMS) accelerometers in smartphones have a high sampling rate and are sensitive to detect the jerks of a ground vehicle when transient events occur (i.e., hitting potholes or bumps) (Bhoraskar et al., 2012; Chen & Guinness, 2014). To distinguish between the acceleration anomaly caused by a transient event and vehicle regular acceleration/deceleration, it would be ideal to reorient smartphone accelerometer to make the smartphone axes align with the vehicle axes, which means the X- and Y-axes of the smartphone directly sense the vehicle's horizontal acceleration/deceleration. On the other

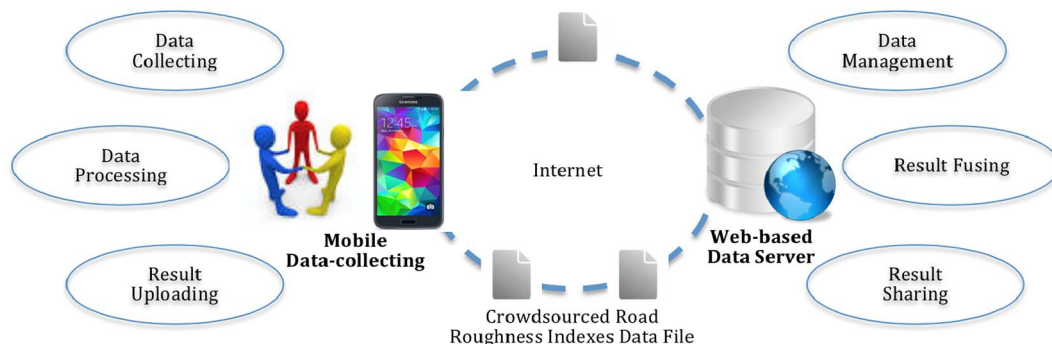


Fig. 1. System architecture.

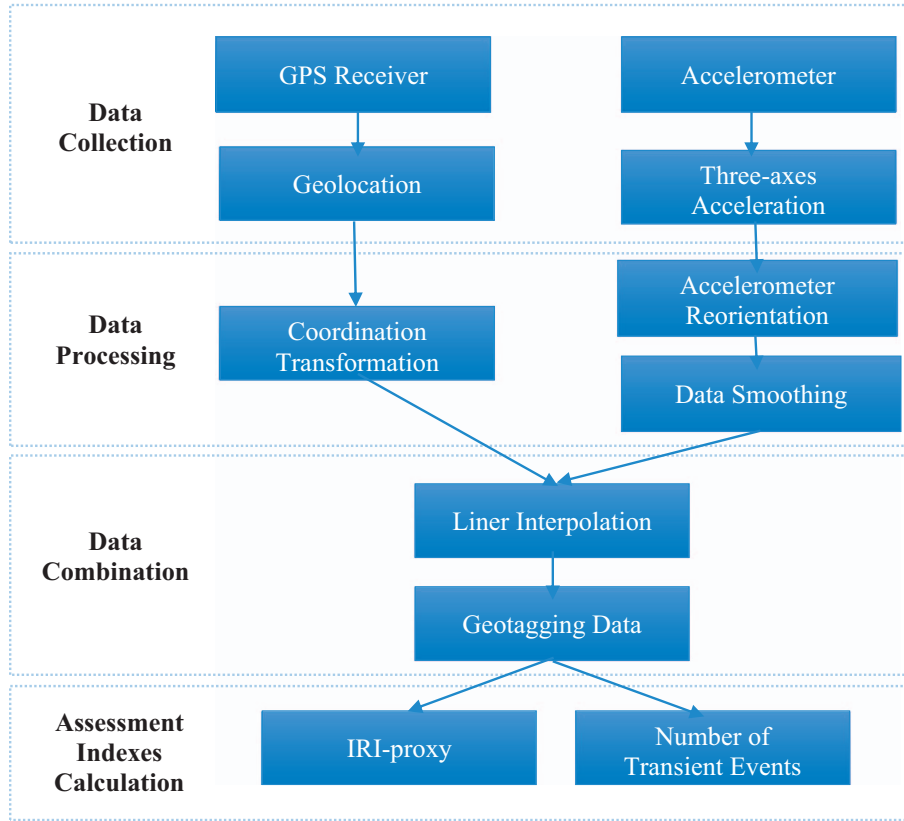


Fig. 2. The flow chart of real-time road surface assessment using smartphone.

hand, Z-axis acceleration, which is perpendicular to the vehicle, can be used to identify the acceleration anomaly caused by vehicle vibration. If the condition is satisfied, the accelerometer is called well-oriented, otherwise disoriented. Eqs. (1)–(4) are adapted from (Astarita et al., 2012), which can be used to perform accelerometer orientation achieved through the Euler Angles.

$$\alpha = \tan^{-1}(a_y'/a_z') \quad \beta = \tan^{-1}(-a_x'/(\sqrt{(a_y')^2 + (a_z')^2})) \quad (1)$$

$$a_{xreor} = \cos(\beta)a_x' + \sin(\beta)\sin(\alpha)a_y' + \cos(\alpha)\sin(\beta)a_z' \quad (2)$$

$$a_{yreor} = \cos(\alpha)a_y' - \sin(\alpha)a_z' \quad (3)$$

$$a_{zreor} = -\sin(\beta)a_x' + \cos(\beta)\sin(\alpha)a_y' + \cos(\beta)\cos(\alpha)a_z' \quad (4)$$

a_x', a_y', a_z' are the three directions' accelerations gathered from a disoriented accelerometer, $a_{xreor}, a_{yreor}, a_{zreor}$ are the reoriented three-axes accelerations. α is the roll angle which shows a rotation around X-axis, β is the pitch angle which shows the rotation around Y-axis.

Fig. 3 illustrates the differences in orientation between a disoriented accelerometer which doesn't match the measurements of the data and the well-oriented accelerometer. After reorientation, the X-axis acceleration is roughly below zero, Y-axis is now at zero, and the Z-axis is now at negative one.

2.2.2. Geotagging data

Accelerometers measure specific force, which is the acceleration relative to free-fall. To extract acceleration signals generated by the road roughness, a high-pass filter as well as a low-pass filter applied to the Z-axis acceleration measurements. The low-pass filter is used to extract the force of Earth gravity from the measured acceleration. Then the high-pass filter is applied to eliminate the contribution of the Earth gravity to obtain a corrected acceleration. Eqs. (5)–(7) are adapted from (SensorEvent, 2017), the low-pass filter is applied as:

$$Y_n = \alpha \cdot Y_{n-1} + (1 - \alpha) \cdot X_n \quad (5)$$

where,

$$\alpha = \frac{t}{t + dT}, \quad (6)$$

t is the current time tag, dT is the event delivery rate, Y_{n-1} is the filtered output of the last epoch, Y_n is the current filtered output, and X_n is the current observation.

Having applied the low-pass filter, the following high-pass filter is used to eliminate the Earth gravity:

$$Z_n = X_n - Y_n = \alpha \cdot X_n - \alpha \cdot Y_{n-1} \quad (7)$$

where Z_n is the corrected acceleration.

The output rate of the built-in GPS receiver (typically 1 Hz) is far lower than the built-in accelerometer (typically 100 Hz). To geo-reference each accelerometer measurement, a linear interpolation scheme is applied, given the hypothesis that the ground vehicle moves with a constant speed between two adjacent GPS positions.

To calculate the distance between two adjacent GPS positions, the original geodetic coordinates are transformed into ECEF (Earth-Centered, Earth-Fixed) coordinates, which are coordinates in a Cartesian coordinate system. Eqs. (8)–(11) are adapted from (Clynch, 2017). Given the geodetic latitude φ , longitude λ , and ellipsoidal height h , where the radius of curvature in the prime vertical, N , is given by:

$$N = \frac{a}{\sqrt{1 - e^2 \sin^2 \varphi}} \quad (8)$$

where the semi-major axis $a = 6,378,137$, the first eccentricity $e = 8.1819190842622 \times 10^{-2}$, then the ECEF coordinates xyz can be obtained with:

$$x = (N + h) \cos \varphi \cos \lambda \quad (9)$$

$$y = (N + h) \cos \varphi \sin \lambda \quad (10)$$

$$z = ([1 - e^2]N + h) \sin \varphi \quad (11)$$

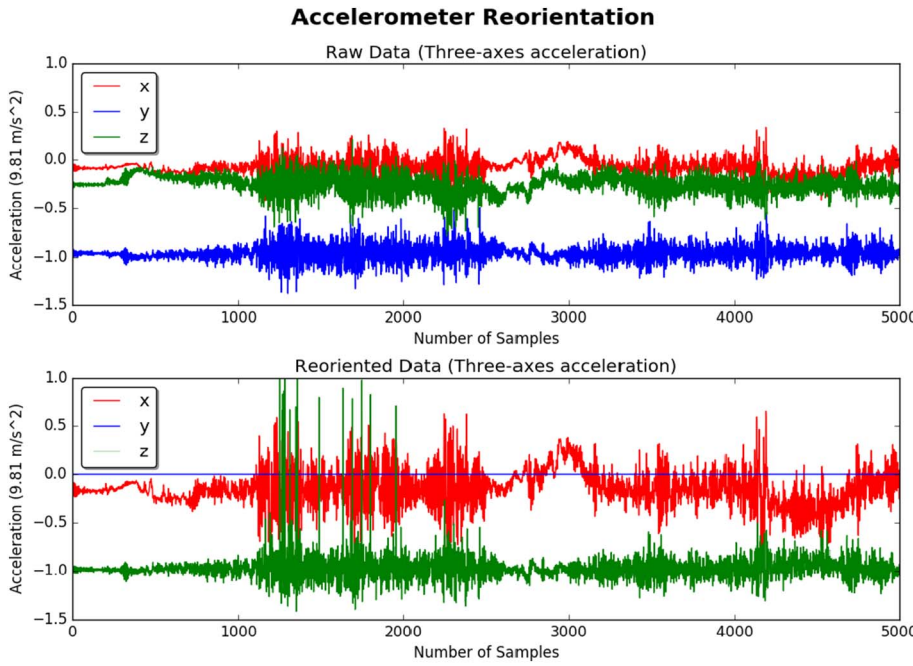


Fig. 3. A comparison between raw data and reoriented data following the reorientation using Euler angles.

Due to the short time interval of 1 s between two GPS sample points, it is reasonable to assume that the velocities of the ECEF coordinate components are constant, therefore, we can apply the following equations to estimate the coordinates of accelerometer measurement sampled at time t :

$$\begin{aligned} x &= x_0 + \frac{(t - t_0)(x_1 - x_0)}{t_1 - t_0} \\ y &= y_0 + \frac{(t - t_0)(y_1 - y_0)}{t_1 - t_0} \\ z &= z_0 + \frac{(t - t_0)(z_1 - z_0)}{t_1 - t_0} \end{aligned} \quad (12)$$

where (x_0, y_0, z_0) and (x_1, y_1, z_1) are the coordinates of two consecutive GPS locations sampled at time t_0 and t_1 , respectively. With the coordinate (x, y, z) , we can then geo-referencing each accelerometer measurement sampled on the roads. The distance S between accelerometer sampled point and the first GPS location (x_0, y_0, z_0) can then be estimated with:

$$S = \sqrt{(x - x_0)^2 + (y - y_0)^2 + (z - z_0)^2} \quad (13)$$

2.2.3. Two road surface condition assessment indexes

Several studies have verified that Z-axis acceleration gathered from smartphones can be used as an effective and reliable signal to estimate road surface condition (Amador-Jiménez & Matout, 2014; Bhoraskar et al., 2012; Harikrishnan & Gopi, 2017). In this study, two assessment indexes are calculated from the geotagged Z-axis acceleration measurements including 1) IRI-proxy for each road segment, and 2) the number of transient events. The IRI-proxy is employed to depict the overall road quality. A transient event occurs when root mean square (RMS) of the Z-axis acceleration exceeds the preset threshold and meets specific criterion that is discussed later. RMS is a statistical measure of the magnitude of a varying quantity. It is especially useful when the function alternates between positive and negative values, e.g., sinusoids. Calculating RMS of Z-axis acceleration can effectively wipe off data noise from signals, smooth the raw data, and highlight the pattern of the vehicle vibration.

IRI-proxy: The International Roughness Index (IRI), which is generally measured by special instruments, is the roughness index commonly used to examine the road surface condition (Sayers & Karamihas,

1998). Since 1986, IRI has been worldwide used as the most common index for examining and evaluating road systems. Some studies indicate that there is a close correlation between IRI and the speed-normalized Z-axis acceleration. Eq. (14) is generated based on (Amador-Jiménez & Matout, 2014). A proxy for IRI (IRI-proxy) can be calculated by multiplying the speed-normalized RMS by 100.

For each road segment, its IRI-proxy can be calculated with:

$$IRI_{proxy} = \frac{n \cdot R}{\sum_{i=1}^n V_i} \cdot 100 \quad (14)$$

where n is the numbers of measurements gathered from a 50-meter road segment, R is the RMS of this road segment, V_i is the real-time speed of the vehicle at the location of the i -th acceleration measurement. Based on the IRI-proxy, the road roughness condition is classified into 4 levels. These four road condition indexes are summarized in Table 2 (Douangphachanh & Oneyama, 2013).

These indexes are generated from the road roughness condition bands used in Lao Road Management System, which contains 6 road condition indexes: 1) Excellent ($0 \leq IRI < 2$), 2) Good ($2 \leq IRI < 4$), 3) Fair ($4 \leq IRI < 7$), Poor ($7 \leq IRI < 10$), 5) Bad ($10 \leq IRI < 18$), and Failed ($IRI \geq 18$) (Douangphachanh & Oneyama, 2013).

Transient Event: Transient events detection is to identify and locate potential potholes/bumps on the road surface (Tan et al., 2014). The vehicle vibration on rough road segments is greater than that on the smooth segments, so transient events are typically represented as events with large amplitude and short wavelength in a RMS curve. Many transient events detection methods have been proposed such as Z-PEAK, Z-DIFF, Z-STDEV et al. (Mednis et al., 2011). Based on the existing methods, an improved method was proposed in this study. Fig. 4 shows the workflow of the proposed transient event detection. It mainly consists of four steps as follows:

Table 2
Four levels of road surface condition based on IRI-proxy.

Road surface condition	IRI-proxy
Excellent/Good	$0 \leq IRI < 4$
Fair	$4 \leq IRI < 7$
Poor	$7 \leq IRI < 10$
Bad/Failed	$IRI \geq 10$

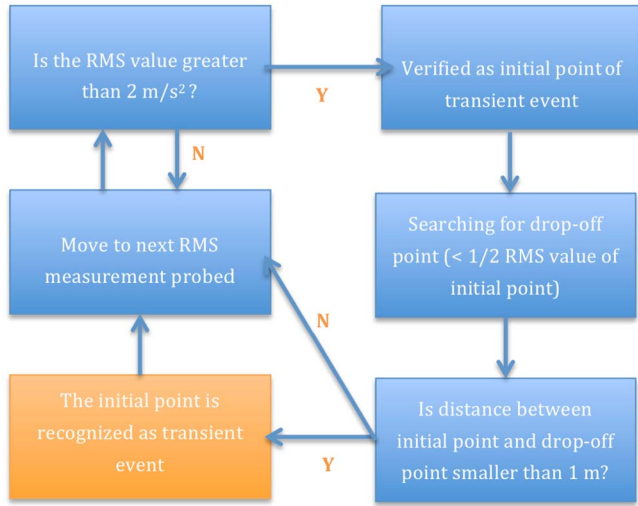


Fig. 4. Workflow of Transient Event Identification.

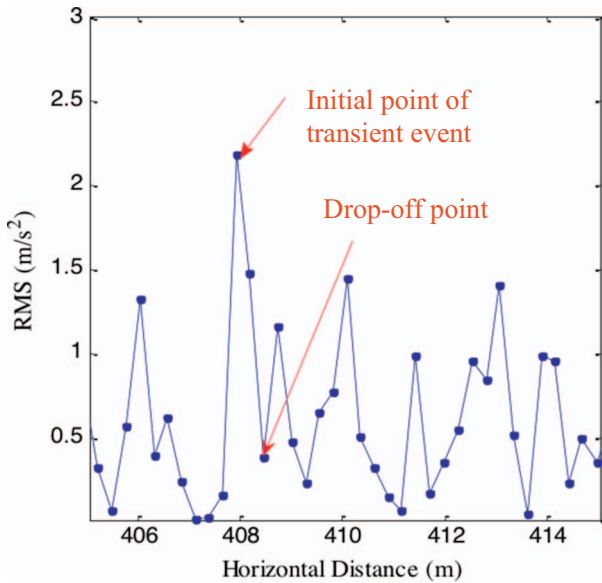


Fig. 5. Illustration of Transient Event Identification along a RMS Curve.

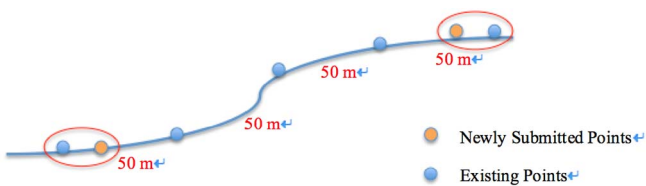


Fig. 6. The process of data synergy from multiple crowdsourcers.

- 1) **Detect the initial point of the transient event:** The search is performed along the RMS curve as shown in Fig. 5. When an RMS value of greater than a preset threshold (through the empirical test, 2 m/s² is set as the threshold value) is detected, an initial point is identified;
- 2) **Detect the drop-off point:** The searching is continued from the initial point until a point with an RMS value of less than half of RMS value of the initial point. If such a point in the RMS curve occurs, a drop-off point is then identified;
- 3) **Transient event validation:** If the distance between the initial point and the drop-off point is < 1 m, a transient event is detected. The threshold value 1 m is selected based on the assumption that the pothole size should be smaller than 1 m.

4) Repeat steps 1–3 from the current point in the RMS curve.

To remove the **anomalous** transient events, two pothole filters are adapted from (Eriksson et al., 2008) and applied as follows:

- 1) **The speed filter:** reject the transient event with zero or very low speed. A threshold of 5 km/h is set to verify each new event.
- 2) **Z-axis acceleration filter:** the events, whose Z-axis acceleration is lower than the threshold of 2 m/s², will be removed.

2.3. Result optimization by integrating crowd sensed data

As each road condition assessment is performed based on the wheel trajectory, which cannot cover the entire pavement, a slight difference exists in the results from different users. This is mainly caused by different driving attempts although the driving routes and vehicles were the same. The detection of the transient events purely relies on where the tire meets the road. For example, a driver may tend to avoid a pothole while another driver may just hit it. Besides, the road surface is a slow, dynamic changing surface. After a long-term use, road surface quality will become worse with more new potholes. Therefore, it is beneficial to take advantages of a crowdsensing solution, which integrates contributions from the public and provides a better assessment of the entire pavement. In this study, a cloud storage service is employed to synergy the contributions from multiple crowdsourcers and publish the integrated results.

Result Optimization: Two data files, one for storing the RMS and IRI-proxy, while the other for transient events, are automatically outputted. The newly submitted data files are processed on the server to optimize and update the crowd sensed road surface conditions.

In this study, the dataset $\text{IRI-proxy} = \{R1, R2, \dots, Rn\}$ represents a set of IRI-proxy values for each 50-meter road segment. For the same road segment, each newly submitted dataset would be merged to the existing dataset as shown in Fig. 6.

A weighting scheme based on the distance between newly submitted points and their nearest existing points is proposed. For each existing point, its IRI-proxy is recalculated based on newly submitted data with:

$$u_i(x) = \frac{w_i(x) \cdot u_i + u_0(x)}{w_i(x) + 1} \quad (15)$$

where,

$$w_i(x) = 1 - \frac{d(x, x_i)}{d} \quad (16)$$

$u_0(x)$ is the original IRI-proxy value at an existing point, $u_i(x)$ is the recalculated IRI-proxy value at an existing point, d is the distance tolerance (50 m, in this study), $d(x, x_i)$ is the distance between a newly reported point x_i and its nearest existing point x , u_i is the IRI-proxy value of the newly submitted point, and $w_i(x)$ is the weight signed to the IRI-proxy value at the newly submitted point.

Numerous studies indicate that the positioning accuracies of the smartphone GPS receivers ranged from 5 to 10 m (Zandbergen, 2009; Zandbergen & Barbeau, 2011). Therefore, the positioning error of detected potholes can be as large as 10 m. For this reason, all potholes within a circle with a radius of 10 m are considered as one pothole. Thus,

- 1) If the distance between the newly detected pothole to its nearest existing pothole is < 10 m, the position of the existing pothole will be recalculated as the average of these two positions;
- 2) If the distance between these two potholes is longer than 10 m, the newly detected pothole will be considered as a new pothole and added to the database.

Furthermore, the server also counts the number of reports for each potential pothole. If a potential pothole has been detected and reported

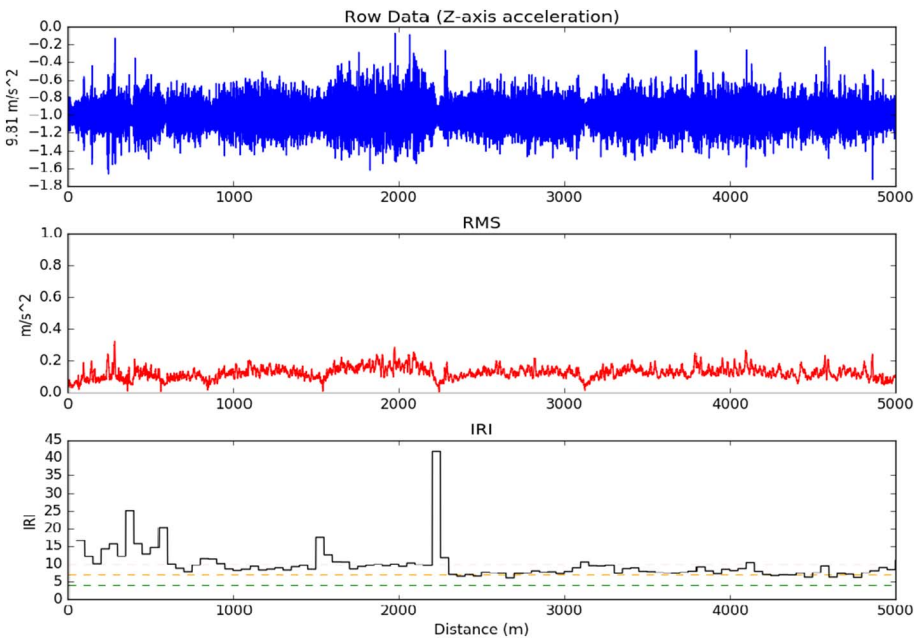
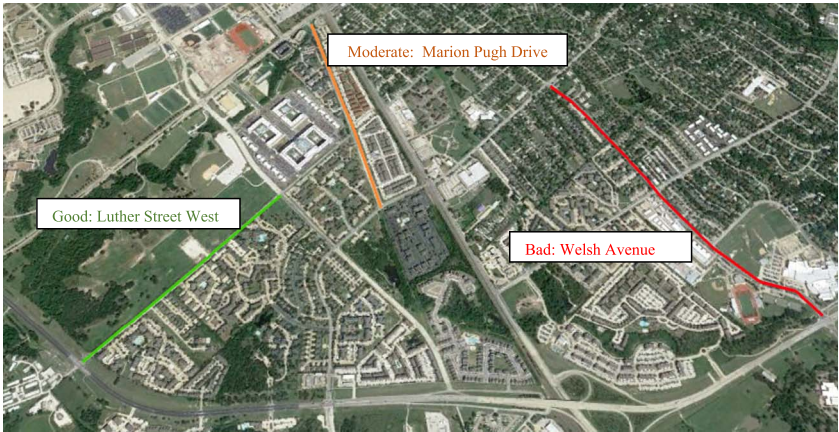


Fig. 7. The raw data, RMS of Raw data, and IRI-proxy of a 5-kilometer road segment.

Table 3
Description of three typical road segments.

	Road name	Length (meter)	Road surface description	Overall condition	Data acquisition time
Segment A	Luther Street West, College Station, TX	1071	Smooth concrete road surface	Good	08/26/2017 4:20 pm
Segment B	Marion Pugh Drive, College Station, TX	1093	Fair good gravel road with some tars on the surface	Moderate	08/26/2017 4:45 pm
Segment C	Welsh Avenue, College Station, TX	1630	Bumpy gravel road surface with several potholes	Bad	08/26/2017 5:10 pm



by three different crowdsourcers, then it will be published. In this way, the accuracy of the crowd sensed results can be improved.

2.4. A cloud-based framework for data visualization and sharing

In this study, a lightweight, cloud-based framework, which takes advantages of free Google services, is developed in the study. Cloud storage services have been widely used by consumers, business and governments to host, manage and collaborate on a huge amount of information. As one of the most popular customer clouds, Google Drive offers users a cost-effective ability to access, host, collaborate on, and disseminate files. Each user is given 15GB of free storage. Google Drive supports users to share their files or folders with individuals and with groups so that they can view, manage and comment on it. In this study,

the administrator builds connections with all crowdsourcers using Google Drive and authorizes them to submit data to our server.

A Cloud Mapping Method - Google Fusion Table is used to map the potholes and road surface conditions in this study. Google Fusion Table is an experimental data visualization web application that allows users to gather, manage, collaborate on, visualize, and publish data tables online (Alon, 2009). Google Fusion Table provides a simple and effective approach, which is accessible to inexperienced users and empowers these users to develop their database-driven web-based application (Warren, 2012). It allows users to map various kinds of features in minutes including points, lines, polygons, customer addresses, and countries. The newly generated map will appear with several small red placemarks based on the location data.

Table 4
The comparison of three typical road segments.

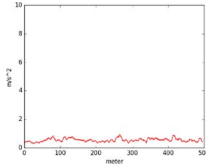
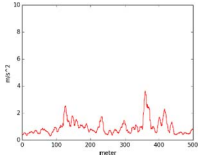
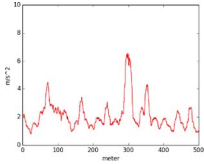
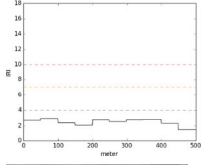
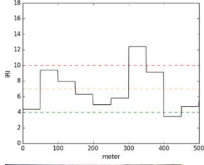
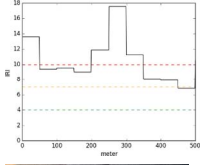



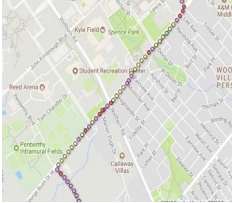
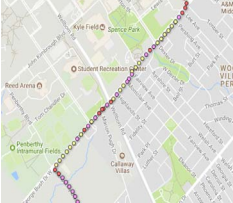
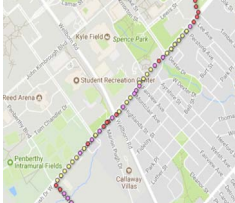
	Segment A	Segment B	Segment C
RMS of Z-acceleration	0.4347 m/s ²	0.9258 m/s ²	2.8826 m/s ²
IRI-proxy	2.5734	7.2624	11.6374
Quality assessment	Good	Poor	Bad
RMS			
IRI			
Road Image			

Table 5
The comparison of three different smartphone models.

	Moto X Pure	iPhone 6	iPhone 7	Standard deviation
RMS mean m/s ²	0.3435	0.3384	0.3291	0.0075
IRI-proxy mean	10.8241	10.8187	10.4341	0.2236
Estimated road surface condition				Data Acquisition Time: 10/13/2017 8:20 AM Location: George Bush Drive, College Station, TX.

3. Experiments and results

This sections covers a brief introduction about the field tests, data analysis, and result integration and visualization.

3.1. Field tests

To verify the proposed solution, some driving tests were carried out on a road segment of about 50 km containing different levels of surface roughness in College Station, Texas. Test data was collected from five different drivers who drove routes for 15 days. The iOS app *Crowdsense*, was installed on 3 iOS phones (i.e., two iPhone 6, one iPhone 7), and the Android app *AndroSensor* was installed on 2 Android phones (i.e., Moto X Pure). All these phones are equipped with a high-sensitivity built-in 3-axis accelerometer and a GPS receiver. Each smartphone was fixed in the car using smartphone holder. The GPS and Z-axis accelerometer data from the smartphones were collected. The smartphones measured acceleration data with an output rate of 100 Hz while generating GPS position information at 1 Hz. In this test, the cars were driven normally, with a maximum speed of approximately 70 km/h. Even at maximum speed, the smartphones could log 5 or 6 acceleration

measurements per meter, which enabled analysis of the road surface roughness with a high spatial resolution. To protect user privacy seriously, all sensed data were completely anonymized. Users' explicit permission is required prior to enabling the sensors.

3.2. Result evaluation

Fig. 7 shows the result of a 5-kilometer road segment. In this figure, the upper subplot shows the raw data, the middle subplot shows RMS of Z-axis acceleration, the lower subplot shows IRI-proxy for every 50-m traveled along the horizontal plane is calculated to indicate the road surface roughness. Three typical road segments (A, B, C) are selected from the testing routes to verify the proposed assessment strategy. A detailed description of these road segments in listed in Table 3. An iPhone 6 smartphone was used to run *Crowdsense* for data collection. This smartphone was fixed in the cabin of a 2009 Toyota Corolla. Statistical results of mean RMS values, IRI-proxy, and road surface images of three road segments (i.e., A, B and C) are presented in Table 4. Segment A, which has the highest road quality, was labeled “Good”. The mean IRI-proxy of Segment A is 2.5734, the mean value of RMS is 0.4347 m/s².

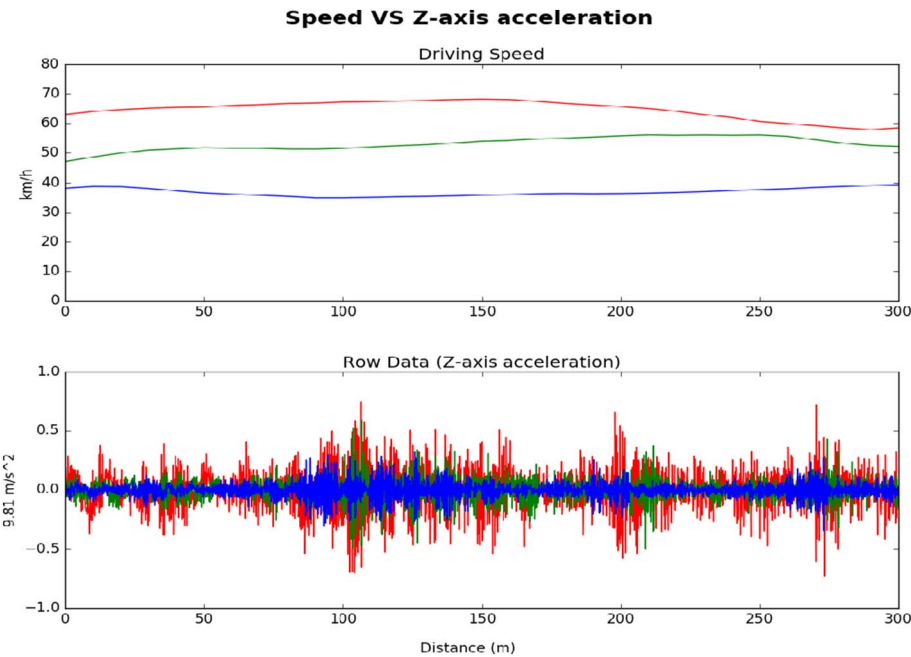


Fig. 8. Three driving speed (Low, Medium, High) with Their Corresponding Z-axis Acceleration Gathered from the Same Road Segment.

Table 6
The comparison of IRI-proxy calculated with different driving speeds.

IRI-Proxy (Low)	IRI-Proxy (Medium)	IRI-Proxy(High)
1.809354497	1.949075566	1.901084422
2.713605347	1.862560789	2.596207585
2.946428568	1.701830928	2.624650091
2.302405857	2.547429886	2.142437912
2.032438854	1.7268601	2.829025458
2.786624122	2.115270482	4.136784105
2.576768388	2.136877558	3.278992175
2.763603782	1.897341655	3.417223982
1.809354497	1.949075566	1.901084422

Segment B, which has a medium-level of road quality, was labeled “Poor” based on the calculated IRI-proxy 7.2624, and with the mean value of RMS is 0.9258 m/s^2 . Segment C, which has the worst road quality, was labeled “Bad”. The mean IRI-proxy of Segment C is 11.6374, with the mean value of RMS is 2.8826 m/s^2 .

Table 5 shows the statistical results of three smartphone models (i.e., Moto X Pure, iPhone 6, iPhone7) under test to illustrate the repeatability by using different smartphones. These three smartphones were fixed on the same car (i.e., 2009 Toyota Corolla) for testing the same road segment (i.e., George Bush Drive, College Station, TX). The differences of the mean RMS and mean IRI-proxy of the above smartphone models are small. The IRI-proxy maps generated based on different phones are all very similar, which indicates that the proposed



Fig. 9. True Pothole Distribution and Four Pothole Detection Methods' Results from 5 Laps. (Red Dot: True pothole; Blue Dot: Detected Pothole; Light Blue Buffer: Positioning Error Tolerance). (For interpretation of the references to color in this figure legend, the reader is referred to the web version of this article.)

Table 7
The performance of four pothole detection method.

False positive rate				
Positioning error tolerance	5 Meters		10 Meters	
Number of laps	5	10	5	10
Z-PEAK	22.22%	17.38%	11.76%	5.88%
Z-DIFF	57.14%	50%	16.66%	10.58%
Z-STEDV	35.29%	23.59%	16.66%	11.11%
IMPROVED	27.27%	16.67%	6.73%	6.14%

Coverage rate				
Positioning error tolerance	5 Meters		10 Meters	
Number of laps	5	10	5	10
Z-PEAK	25.92%	37.03%	40.74%	62.06%
Z-DIFF	37.04%	51.85%	66.67%	81.84%
Z-STEDV	59.25%	74.07%	77.78%	85.18%
IMPROVED	62.96%	88.89%	88.89%	92.59%

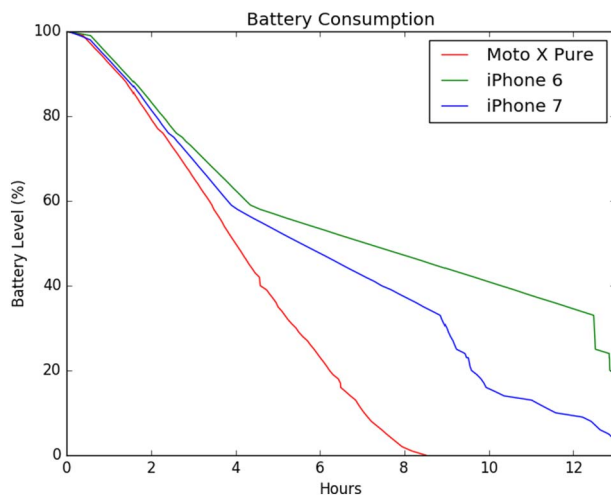


Fig. 10. Battery consumption test.

approach is suitable for different phone models.

Studies have demonstrated Z-axis acceleration is influenced by the driving speed (Lima et al., 2016). To test the relationship between the driving speed with Z-axis acceleration, Road segment A was tested three times at different driving speeds: low (30–40 km/h), medium (40–50 km/h), high (50–60 km/h). Fig. 8 shows three different driving speeds and their corresponding Z-axis acceleration. This figure indicates that the high driving speed will increase the vibration of Z-axis acceleration. The IRI-proxy was calculated three times based on the datasets gathered with different driving speed detailed in Table 6. The table indicates that these three tests' results are similar, just one 50-meter "Good" road segment was mislabeled as "Fair". It indicates that the proposed speed-normalized method could handle the data difference which is caused by the different driving speed.

To verify the accuracy of proposed crowdsensing solution for the pothole detection, a road test was carried out in Texas A&M University Parking Lot 50, where contains a lot distinguishable potholes. The test was repeated 10 times by a tester with different smartphones for data collection. Four pothole detection methods: Z-PEAK, Z-DIFF, Z-STEDV and the method we proposed are respectively utilized to extract and label potholes. The true pothole number is 28, which were manually counted prior to the test. Half-meter-accuracy positions of these 28 potholes were geotagged by using a hand-held GPS.

The performance of Z-PEAK, Z-DIFF, Z-STEDV and the proposed

crowdsensing solution was evaluated by comparing the truth reference with their results from five laps and the results from ten laps from two respects: 1) coverage rate (#correctly detected potholes/#true pothole); 2) false positive rate (#mislabel potholes/#detected potholes). Fig. 9 shows the true potholes distribution (red dots) and 4 different methods' pothole detection results from five laps (blue dots). The positioning error tolerance is set as 5 m (light blue buffer) in this figure, which means the detected pothole with a distance < 5 m from the nearest true pothole, is judged as a correct detection.

Table 7 details the false positive rates and the coverage rates of these four methods gathered from five laps and ten laps. Two positioning error tolerances (5 m and 10 m) are respectively adapted for the detection performance evaluation. The test indicates that Z-Peak has a high accuracy for pothole detection. However, the coverage rate of Z-Peak method is the lowest. Another two pothole detection algorithms (Z-DIFF and Z-STEDV) which are low in detection accuracy and coverage rate compared to the improved algorithm. The improved algorithm does a better job of properly detecting potholes by integrating crowd sensed data, increasing the coverage rate and lowering the false positive rate of the pothole detection.

Battery consumption is an important issue for crowdsensing. In this study, battery consumption of different phones (i.e., Moto X Pure, iPhone 6, and iPhone 7) was also tested as shown in Fig. 10. The sampling rate of accelerometers was set to 100 Hz and GPS receivers were enabled for all three phones. The result shows that the battery of Android-based Moto X Pure can offer 8–9 h of data collection. iPhone 6 and iPhone 7 can support > 12 h data collection. To date, several studies (Ben Abdesslem, Phillips, & Henderson, 2009; Constandache, Gaonkar, Sayler, Choudhury, & Cox, 2009; Peng et al., 2017; Wang, Tang, Xue, & Yang, 2017; Zhuang, Kim, & Singh, 2010) have been carried out, which can effectively minimize the energy consumption of built-in smartphone sensors. In the future study, a more energy-efficient crowdsensing system will be built by taking advantages of the former studies, choosing more appropriate sampling rate of sensors, and optimizing algorithms.

As mentioned above, the contribution from crowdsourcers were mapped using Google Fusion Table. Three maps, as shown in Fig. 11, were generated from the 15-day detection data to depict road surface condition. Fig. 11-A presents pothole distribution. The pothole density map was obtained by enabling the heat map layer as shown in Fig. 11-B. Meanwhile, Fig. 11-C shows the overall road roughness map based on IRI-proxy, in which each point was colored based on its IRI-proxy. In this map, "Good" in yellow, "Fair" in Green, "Poor" in purple, and "Bad" in red. These three maps give the public a clear view of the most up-to-date road surface condition for some road segments in College Station, Texas.

4. Discussion and conclusion

In the study, a labor-saving and low-cost crowdsensing system for road surface condition assessment was introduced, and it has verified the feasibility of using built-in smartphone sensors for road surface condition assessment in terms of two detection indexes: IRI-proxy and the number of the transient events. In order to examine the proposed solution, test data were collected from five users driving routes around College Station, Texas. The drivers drove 50 km road segments with different surface roughness levels. The field tests demonstrated that the built-in smartphone sensors can effectively assess road quality and detect the transient events. The overall road surface condition can be accurately judged and labeled by the IRI-proxy and the transient events can be efficiently identified. By implementing a crowdsensing solution, the road surface condition can be constantly monitored. Meanwhile, the most up-to-date and more accurate assessment results were achieved by mining crowd sensed data. What's more, the Google Fusion Table can offer powerful access for data management and visualization.

However, it has shown that using different devices in different

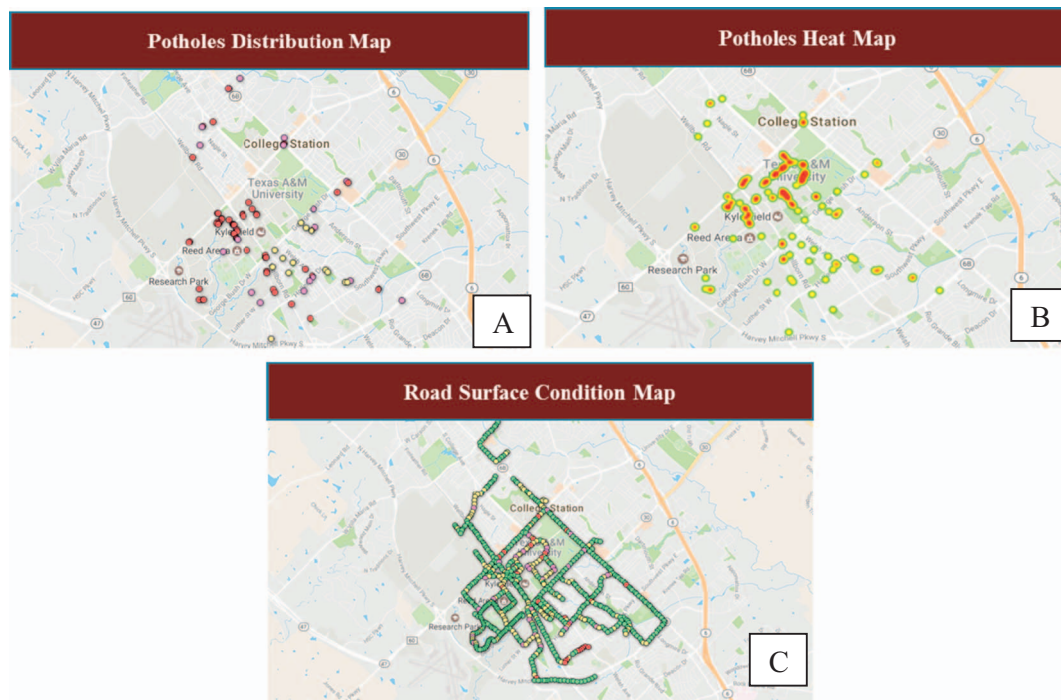


Fig. 11. Road surface roughness maps (A: potholes distribution map, B: potholes density map, C: IRI-proxy map).

driving attempts can generate different assessment results, even though they were carried out on the same routes. It is mainly because ground vehicles always move in a line-scan rather than area-scan pattern. Due to the limited accuracy of the built-in smartphone GPS receiver, a high-accuracy positioning result cannot be guaranteed. “How accurate are smartphone GPS receivers?” is the most often asked question related to crowdsensing. The positioning accuracy of smartphones has been significantly enhanced over the past decade. Zandbergen (2009) examined the positioning accuracy of the 3G iPhone - the first mobile device which integrates three different positioning technologies. The result indicates an average positioning accuracy is 8 m. In Zandbergen and Barbeau (2011), the result shows the positioning accuracy of smartphones has been improved to 5–8 m, which is sufficient for most location-based services. Chen et al. (2014) proposed a novel “DGNSS-C” algorithm which can enhance the positioning accuracy of smartphones by 30%–40% (2–3 m). Pesyna Jr, Heath Jr, and Humphreys (2014) created a “centimeter-accurate” mobile system by combining the GPS recordings with a smartphone-quality Global Navigation Satellite System antenna. The latest news published on IEEE SPECTRUM (Samuel, 2017) said Broadcom Limited (a global semiconductor leader) designed a more accurate GPS chip (BCM47755), which enables 30-centimeter positioning accuracy and 50% less battery drain for the next generation of smartphones releasing in 2018.

With the rapid development of the modern smartphone technologies and the increasing number of public crowdsensing smartphone participants, the proposed solution is promising for providing accurate real-time road surface roughness information and offering comprehensive and timely road service information to road maintenance works as well as drivers.

References

- Aleadelat, W., & Ksaibati, K. (2017). Estimation of pavement serviceability index through android-based smartphone application for local roads. *Transportation Research Record*, 2639, 129–135. <http://dx.doi.org/10.3141/2639-16>.
- Allouch, A., Koubaa, A., Abbes, T., & Ammar, A. (2017). RoadSense: smartphone application to estimate road conditions using accelerometer and gyroscope. *IEEE Sensors Journal*, 17(13), 4231–4238. <http://dx.doi.org/10.1109/jsen.2017.2702739>.
- Alon, H. (2009, June 09). Google fusion tables. Retrieved October 13, 2017, from [https://](https://research.googleblog.com/2009/06/google-fusion-tables.html)

- research.googleblog.com/2009/06/google-fusion-tables.html.
- Amador-Jiménez, L., & Matout, N. (2014). A low cost solution to assess road's roughness surface condition for pavement management. *Transportation research board 93rd annual meeting (no. 14-3086)*<http://docs.trb.org/prp/14-3086.pdf>.
- Astarita, V., Caruso, M. V., Danieli, G., Festa, D. C., Giofrè, V. P., Iuele, T., & Vaiana, R. (2012). A mobile application for road surface quality control: UNiquAlroad. *Procedia - Social and Behavioral Sciences*, 54, 1135–1144. <http://dx.doi.org/10.1016/j.sbspro.2012.09.828>.
- Ben Abdesslem, F., Phillips, A., & Henderson, T. (2009, August). Less is more: Energy-efficient mobile sensing with senseless. *Proceedings of the 1st ACM workshop on networking, systems, and applications for mobile handhelds* (pp. 61–62). ACM. <http://dx.doi.org/10.1145/1592606.1592621>.
- Beuving, E., De Jonghe, T., Goos, D., Lindahl, T., & Stawarski, A. (2004). Environmental impacts and fuel efficiency of road pavements. *European Roads Review*, 2^{http://www.eapa.org/usr_img/position_paper/fuel_efficiency_report.pdf}.
- Bhoraskar, R., Vankadhara, N., Raman, B., & Kulkarni, P. (2012). Wolverine: Traffic and road condition estimation using smartphone sensors. *2012 Fourth international conference on communication systems and networks (COMSNETS 2012)*<http://dx.doi.org/10.1109/comsnets.2012.6151382>.
- Cao, Y., Labuz, J., & Guzina, B. (2011). Evaluation of pavement system based on ground-penetrating radar full-waveform simulation. *Transportation Research Record*, 2227, 71–78. <http://dx.doi.org/10.3141/2227-08>.
- Chen, K., Lu, M., Tan, G., & Wu, J. (2013). CRSM: crowdsourcing based road surface monitoring. *2013 IEEE 10th international conference on high performance computing and communications & 2013 IEEE international conference on embedded and ubiquitous computing*<http://dx.doi.org/10.1109/hpcc.and.euc.2013.308>.
- Chen, R., & Guinness, R. (2014). Geospatial computing in mobile devices. *Artech House*, 1–8 (Chapter 1).
- Chen, R. Z., Chu, T. X., Liu, J. B., Li, X., Chen, Y., & Chen, L. (2014). DGNSS-C: A differential solution for enhancing smartphone GNSS performance. *Proceedings of the ION GNSS* (pp. 490–497).
- Clynch, J. R. (2017). Geodetic coordinate conversions I. *Geodetic to/from geocentric latitude*. Retrieved October 14, 2017, from <http://clynchg3c.com/Technote/geodesy/coordcv.pdf> (n.d.).
- Constandache, I., Gaonkar, S., Sayler, M., Choudhury, R. R., & Cox, L. (2009). EnLoc: Energy-efficient localization for mobile phones. *IEEE INFOCOM 2009 — The 28th conference on computer communications*<http://dx.doi.org/10.1109/infcom.2009.5062218>.
- Das, T., Mohan, P., Padmanabhan, V. N., Ramjee, R., & Sharma, A. (2010). PRISM. *Proceedings of the 8th international conference on Mobile systems, applications, and services — MobiSys '10* ACM Press<http://dx.doi.org/10.1145/1814433.1814442>.
- Douangphachanh, V., & Oneyama, H. (2013). A study on the use of smartphones for road roughness condition estimation. *Journal of the Eastern Asia Society for Transportation Studies*, 10, 1551–1564. <http://dx.doi.org/10.11175/easts.10.1551>.
- Eriksson, J., Girod, L., Hull, B., Newton, R., Madden, S., & Balakrishnan, H. (2008). The pothole patrol. *Proceeding of the 6th international conference on Mobile systems, applications, and services — MobiSys '08* ACM Press<https://doi.org/10.1145/1378600.1378605>.
- Harikrishnan, P. M., & Gopi, V. P. (2017). Vehicle vibration signal processing for road

- surface monitoring. *IEEE Sensors Journal*, 17(16), 5192–5197. <http://dx.doi.org/10.1109/jsen.2017.2719865>.
- Harrison, F., & Park, H. (2008). Comparative performance measurement: Pavement smoothness. *NCHRP 20-24 (37B) final rep.* Washington, DC: National Cooperative Highway Research Program, Transportation Research Board.
- Kim, Y. R. (2001). *Assessing pavement layer condition using deflection data (No. 254)*. Transportation Research Board, National Research Council.
- Lima, L. C., Amorim, V. J. P., Pereira, I. M., Ribeiro, F. N., & Oliveira, R. A. R. (2016, November). Using crowdsourcing techniques and mobile devices for asphaltic pavement quality recognition. *Computing systems engineering (SBESC), 2016 VI Brazilian symposium on (pp. 144–149)*IEEE<http://dx.doi.org/10.1109/sbesc.2016.029>.
- Macias, E., Suarez, A., & Lloret, J. (2013). Mobile sensing systems. *Sensors*, 13(12), 17292–17321. <http://dx.doi.org/10.3390/s131217292>.
- Mednis, A., Strazdins, G., Zviedris, R., Kanonirs, G., & Selavo, L. (2011). Real time pothole detection using Android smartphones with accelerometers. *2011 International conference on distributed computing in sensor systems and workshops (DCOSS)IEEE*<http://dx.doi.org/10.1109/dcoos.2011.5982206>.
- Paterson, W., & Attoh-Okine, B. (1992). Summary models of paved road deterioration based on HDM-III. *Transportation Research Record*, 1344.
- Peng, J., Zhu, Y., Zhao, Q., Zhu, H., Cao, J., Xue, G., & Li, B. (2017). Fair energy-efficient sensing task allocation in participatory sensing with smartphones. *The Computer Journal*, 60(6), 850–865. <http://dx.doi.org/10.1093/comjnl/bxx015>.
- Perttunen, M., Mazhelis, O., Cong, F., Kaupila, M., Leppänen, T., Kantola, J., ... Riekk, J. (2011). Distributed road surface condition monitoring using mobile phones. *Ubiquitous intelligence and computing (pp. 64–78)*Berlin Heidelberg: Springer. http://dx.doi.org/10.1007/978-3-642-23641-9_8.
- Pesyna, K. M., Jr., Heath, R. W., Jr., & Humphreys, T. E. (2014). Centimeter positioning with a smartphone-quality GNSS antenna. *Proceedings of the ION GNSS + Meeting*<http://radionavlab.ae.utexas.edu/images/stories/files/papers/ion2014Pesyna.pdf>.
- Samuel, K. M. (2017, September 21). *Generate APA citations for websites*. Retrieved October 13, 2017, from Superaccurate GPS Chips Coming to Smartphones in 2018.
- Sayers, M. W., & Karamihas, S. M. (1998). *The little book of profiling*. Ann Arbor, MI: The University of Michigan Transportation Research Institute (UMTRI).
- SensorEvent (2017, July 24). Retrieved October 13, 2017, from. <https://developer.android.com/reference/android/hardware/SensorEvent.html>.
- Singh, G., Bansal, D., Sofat, S., & Aggarwal, N. (2017). Smart patrolling: An efficient road surface monitoring using smartphone sensors and crowdsourcing. *Pervasive and Mobile Computing*, 40, 71–88. <http://dx.doi.org/10.1016/j.pmcj.2017.06.002>.
- Tan, G., Lu, M., Jiang, F., Chen, K., Huang, X., & Wu, J. (2014). Bumping: A bump-aided inertial navigation method for indoor vehicles using smartphones. *IEEE Transactions on Parallel and Distributed Systems*, 25(7), 1670–1680. <http://dx.doi.org/10.1109/tpps.2013.194>.
- Vittorio, A., Rosolino, V., Teresa, I., Vittoria, C. M., Vincenzo, P. G., & Francesco, D. M. (2014). Automated sensing system for monitoring of road surface quality by mobile devices. *Procedia - Social and Behavioral Sciences*, 111, 242–251. <http://dx.doi.org/10.1016/j.sbspro.2014.01.057>.
- Wang, J., Tang, J., Xue, G., & Yang, D. (2017). Towards energy-efficient task scheduling on smartphones in mobile crowd sensing systems. *Computer Networks*, 115, 100–109. <http://dx.doi.org/10.1016/j.comnet.2016.11.020>.
- Warren, S. (2012, June 26). Introducing new fusion tables API. Retrieved October 13, 2017, from <https://research.googleblog.com/search/label/Fusion%20Tables>.
- Watanatada, T. (1987). *The highway design and maintenance standards model: User's manual for the HDM-III model (Vol. 2)*. Johns Hopkins University Press.
- Xu, B., Ranji Ranjithan, S., & Richard Kim, Y. (2002). New relationships between falling weight deflectometer deflections and asphalt pavement layer condition indicators. *Transportation Research Record*, 1806, 48–56. <http://dx.doi.org/10.3141/1806-06>.
- Zandbergen, P. A. (2009). Accuracy of iPhone locations: A comparison of assisted GPS, WiFi and cellular positioning. *Transactions in GIS*, 13, 5–25. <http://dx.doi.org/10.1111/j.1467-9671.2009.01152.x>.
- Zandbergen, P. A., & Barbeau, S. J. (2011). Positional accuracy of assisted GPS data from high-sensitivity GPS-enabled mobile phones. *Journal of Navigation*, 64(3), 381–399. <http://dx.doi.org/10.1017/s0373463311000051>.
- Zhuang, Z., Kim, K.-H., & Singh, J. P. (2010). Improving energy efficiency of location sensing on smartphones. *Proceedings of the 8th international conference on Mobile systems, applications, and services — MobiSys '10*ACM Press<http://dx.doi.org/10.1145/1814433.1814464>.